

Low mass strange stars and the compact star 1E1207.4-5209

F. I. M. Pereira*

Observatório Nacional, MCTI, Rua Gal. José Cristino 77, 20921-400 Rio de Janeiro RJ, Brazil

(Dated: September 1, 2020)

We study the anomalous mass defects in the first (ascendant) branch of stellar sequences of static strange stars. We employ the nonperturbative equation of state derived in the framework of the Field Correlator Method to describe the hydrostatic equilibrium of the strange matter. The large distance static $q\bar{q}$ potential V_1 and the gluon condensate G_2 are the model parameters that characterize the equation of state.

An attempt is made to determine, from the surface gravitational redshift measurements, the ratio $(\mathcal{P}/\mathcal{E})_C$ at the center of strange stars. For $V_1 = 0$ and $G_2 \gtrsim 0.035 \text{ GeV}^4$, it is shown that $(\mathcal{P}/\mathcal{E})_C \simeq 0.262$ and the corresponding redshift $z_S \simeq 0.47$ are limiting values, at the maximum mass of the stellar sequence. As a direct application of our study, we try to determine the values of V_1 and G_2 from astrophysical observations of the compact star 1E1207.4-5209. After two attempts to obtain the model parameters, our findings show that $V_1 = 0.44 \pm 0.10 \text{ GeV}$ and $G_2 = 0.008 \pm 0.001 \text{ GeV}^4$ in the first attempt and $V_1 = 0.43 \pm 0.085 \text{ GeV}$ and $G_2 = 0.0093 \pm 0.00092 \text{ GeV}^4$ in the second attempt. The corresponding ratios $(\mathcal{P}/\mathcal{E})_C$ are $0.073_{+0.024}^{+0.029}$ and 0.087 ± 0.028 , respectively. As a consequence of these high values of the model parameters, the respective anomalous mass defect of 1E1207.4-5209 are $|\Delta_2 M| \simeq 2.56 \times 10^{53} \text{ erg}$ and $|\Delta_2 M| \simeq 2.94 \times 10^{53} \text{ erg}$.

* flavio@on.br, fimpjm@gmail.com

I. INTRODUCTION

The possibility of anomalous mass defects in compact stars goes back to the works of V. A. Ambartsumyan, G. S. Saakyan and Yu. L. Vartanyan in Refs. [1–5]. Anomalous mass defects would occur at internal stellar densities many times greater than nuclear ($\varepsilon_0 \simeq 0.14 \text{ GeV fm}^{-3}$). Such stellar configurations, in the presence of external perturbations, would undergo transitions of explosive character, from a metastable state to a stable state, with great amounts of liberated energy. The authors considered the superdense stellar matter made of a degenerate gas comprising neutrons, protons, hyperons and electrons, at zero temperature. The baryons being made of quarks, it would be natural to expect unbound quarks to exist in the interior of hyperdense stars. The possibility of hypothetical compact stars made of pure quark matter was then considered by N. Itoh in Ref. [6]. Since the Bodmer-Terazawa-Witten conjecture in Refs. [7–9] the existence of the strange quark matter (SQM), made of an equal number of up, down and strange quarks, has been subject of a lot of theoretical studies, experimental investigations in terrestrial laboratories, and observational studies of astrophysical phenomena.

The properties of SQM in the phase diagram, at small temperatures and large densities, were not completely known due to the nonperturbative character of quantum chromodynamics (QCD). Withing this scenario, the MIT Bag Model became one of the most successful phenomenological models for quark confinement to treat the cold matter at finite chemical potentials and describe the properties of strange stars (see Refs. [10–12]). However, the model has the disadvantage in that the quarks are free particles inside the bag that simulates the confinement; but for larger distances, when the confining forces becomes important, it does not naturally include the confinement from first principles. On the other hand, additional complications appear when magnetic field is taken into account. In a recent work, the SQM in strong magnetic field was considered by the authors of Ref. [13] by using the Richardson potential [14] in which the asymptotic freedom and confinement are built in.

Despite the highly nonlinear character of QCD, the inherent difficulties were overcome by the more recent appearance of the nonperturbative equation of state derived, from first principles, in the framework of the Field Correlator Method (FCM) in Ref. [15]. The great advantage of the model is that it covers the entire phase diagram plane from high temperatures and low densities to low temperatures and high densities. We studied the general

aspects of (normal and anomalous) mass defects of strange stars within the FCM approach in Ref. [16]. We carried out the calculation of the mass defects specially at the maximum masses of the stellar sequences.

In the present article, we study the anomalous mass defects of nonrotating strange stars, without magnetic field and crust (to be considered, in the FCM approach, in future works which are now in progress), within the same lines of our previous investigation. We start the work by studying the anomalous mass defects in the first (ascendant) branches of the stellar sequences, which also includes the region of low mass stars. Then, we use the solutions of the Tolmann-Oppenheimer-Volkov (TOV) equations for the case of constant energy density (see Ref.: [17]) to guide our investigation. In this case, the ratio pressure-to-energy density, $\mathcal{P}_C/\mathcal{E}_C$, at the center of a star can be expressed in terms of the surface or gravitational redshift (henceforth called redshift) of a radiation emitted at a given frequency from the star surface. We extend this simple idea to find an analogous description for the general case of stars with non-constant energy density profiles. The new description is used to determinate the QCD parameters V_1 and G_2 from the astrophysical observation of the compact star 1E1207.4-5204.

The present paper is organized as follows. In Sec. II we introduce the FCM main equations to be used in our calculation. In Sec. III we present the equations needed to describe the stellar configurations: mass defects, hydrostatic equilibrium equations, and the constant energy density solution of TOV equations. Sec. IV is devoted to the non-constant energy density profile inside strange stars. In Sec. V, we made an attempt to estimate the model parameters V_1 and G_2 from the observations of the compact star 1E1207.4-5209. Sec. VI is dedicated to the final remarks.

II. THE NONPERTURBATIVE EQUATION OF STATE AT ZERO TEMPERATURE

Let us summarize the main equations concerning the FCM thermodynamics of quarks (see Refs. [16, 18, 19] for a more detailed description). The main parameters of the non-perturbative equation of state are the large distance static $q\bar{q}$ potential V_1 and the gluon condensate G_2 . For constant V_1 , the pressure, energy density and number density of a (one flavor) quark gas at $T = 0$ are given by

$$p_q^{SLA} = \frac{N_c}{3\pi^2} \left\{ \frac{k_q^3}{4} \sqrt{k_q^2 + m_q^2} - \frac{3}{8} m_q^2 \left[k_q \sqrt{k_q^2 + m_q^2} - m_q^2 \ln \left(\frac{k_q + \sqrt{k_q^2 + m_q^2}}{m_q} \right) \right] \right\}, \quad (1)$$

$$\begin{aligned} \varepsilon_q^{SLA} = & \frac{N_c}{\pi^2} \left\{ \frac{k_q^3}{4} \sqrt{k_q^2 + m_q^2} + \frac{m_q^2}{8} \left[k_q \sqrt{k_q^2 + m_q^2} - m_q^2 \ln \left(\frac{k_q + \sqrt{k_q^2 + m_q^2}}{m_q} \right) \right] \right. \\ & \left. + \frac{V_1}{2} \frac{k_q^3}{3} \right\} \end{aligned} \quad (2)$$

and

$$n_q^{SLA} = \frac{N_c}{\pi^2} \frac{k_q^3}{3}, \quad (3)$$

where

$$k_q = \sqrt{(\mu_q - V_1/2)^2 - m_q^2}, \quad (q = u, d, s), \quad (4)$$

$N_c = 3$ is the color number, and $m_u = 5$ MeV, $m_d = 7$ MeV and $m_s = 150$ MeV are the quark masses. The additional term $(V_1/2)k_q^3/3$ in Eq.(2) comes from the large distance static $q\bar{q}$ potential V_1 .

The total pressure and energy density, including electrons are given by

$$p = \sum_{q=u,d,s} p_q^{SLA} - \Delta|\varepsilon_{\text{vac}}| + p_e, \quad (5)$$

$$\varepsilon = \sum_{q=u,d,s} \varepsilon_q^{SLA} + \Delta|\varepsilon_{\text{vac}}| + \varepsilon_e, \quad (6)$$

where

$$\Delta|\varepsilon_{\text{vac}}| = \frac{11 - \frac{2}{3}N_f}{32} \Delta G_2, \quad (7)$$

is the vacuum energy density difference between confined and deconfined phases (which from now on will be called vacuum energy density), N_f is the number of flavors, and $\Delta G_2 \simeq \frac{1}{2}G_2$ is the difference between the values of the gluon condensate G_2 at $T < T_c$ and $T > T_c$ (T_c is the critical temperature) prescribed by lattice calculations in the Refs. [20, 21]. The numerical equivalence for the MIT Bag Model is made by taking $\Delta|\varepsilon_{\text{vac}}| = B$ and $V_1 = 0$. However, we must have in mind that $\Delta|\varepsilon_{\text{vac}}|$ is a nonperturbative quantity. The corresponding equations for the degenerate electron gas are obtained from Eqs. (1)-(3) by making the changes: $N_c \rightarrow 1$, $V_1 \rightarrow 0$, $\mu_q \rightarrow \mu_e$ and $m_q \rightarrow m_e$.

III. STELLAR CONFIGURATIONS

Stellar configurations are calculated by numerical integration of the hydrostatic equilibrium equations of Tolman-Oppenheimer-Volkov [17, 22] (we come back to these equations in Sec. III B). Of special importance is the total gravitational mass of a compact star (see [23] for details),

$$M = \int_0^R \varepsilon(r) dv(r), \quad (8)$$

where $dv(r) = 4\pi r^2 dr$, which is the mass that governs the Keplerian orbital motion of the distant gravitating bodies around it, as measured by external observers. The baryonic mass (also called rest mass) of a star is $M_A = m_A N_A$, where m_A is the mass per baryon of the baryonic specie A , with the number of baryons given by

$$N_A = \int_0^R n_A(r) e^{\lambda(r)} dv(r), \quad (9)$$

where $e^{\lambda(r)} = [1 - 2GM(r)/(c^2 r)]^{-1/2}$ is the spatial function of the metric; $M(r)$ is the mass within a sphere of radius r , and

$$n_A = \frac{1}{3} \sum_{q=u,d,s} n_q^{SLA} = \frac{1}{3} (n_u^{SLA} + n_d^{SLA} + n_s^{SLA}) \quad (10)$$

is the equivalent baryon number density. The baryonic mass is the mass that the star would have if its baryon content were dispersed at infinity, with zero kinetic energy. In the case of strange stars (because of the quark confinement), N_A is the equivalent number of baryons (not quarks). We here assume $m_A = m_n$ as in our previous works.

A. Mass defects

With the masses M and M_A known, we are in a position to calculate the mass defect (which in our notation¹ is minus the binding energy E_b defined in Refs. [22, 23]) is given by

$$\Delta_2 M = M_A - M. \quad (11)$$

It corresponds to the energy released to aggregate from infinity the dispersed baryonic matter. A stellar configuration is stable if $\Delta_2 M > 0$ (normal mass defect). It is unstable

¹ We here follow the notation according to Refs. [1, 2, 4, 24, 25]

if $\Delta_2 M < 0$ (anomalous mass defect); in this later case, the stellar configuration has an excess of energy with respect to the energy it would have to be a bound system. The star is in a metastable state which means that it might explode or implode in the presence of an external perturbation.

In order to consider the general aspects of the anomalous mass defects, let us write the differential elements of the total gravitational mass, the equivalent number of baryons, and the baryonic (or rest) mass given by

$$dM(r) = \varepsilon dv(r) \quad (12)$$

$$dN_A(r) = n_A(r) e^{\lambda(r)} dv(r) \quad (13)$$

$$dM_A(r) = m_A dN_A(r). \quad (14)$$

Then we find that

$$\begin{aligned} \frac{dM(r)}{dN_A(r)} &= \frac{\varepsilon(r)}{n_A(r)} e^{-\lambda(r)} \\ &= m(r) \sqrt{1 - 2 \frac{G M(r)}{c^2 r}}. \end{aligned} \quad (15)$$

We call $m(r) \equiv \varepsilon(r)/n_A(r)$ the mass-energy per baryon inside the star. On the surface of the star (by taking into account that $e^{-\lambda_R} = e^{\phi_R}$ at $r = R$) Eq. (15) becomes

$$\begin{aligned} \left. \frac{dM(r)}{dN_A(r)} \right|_{r=R} &= m_R e^{\phi_R} \\ &= m_R \sqrt{1 - 2 \frac{G M}{c^2 R}}, \end{aligned} \quad (16)$$

where ϕ is the temporal function of the metric, $m_R \equiv m(R)$ and $M \equiv M(R)$ given by Eq. (8).

In Fig. 1, the panel (a) shows the general features of the stellar sequence for the given values of the parameters V_1 and G_2 . The label **3** (in the first branch) indicates an intermediate point around $0.5M_\odot$ in the low mass region, where the mass defect is anomalous (more visible in panels (b) and (c)). In panel (b), the slope of the M vs. N_A curve at the point **3** given by Eq. (16) and that of the M_A vs. N_A curve are parallel, which means that

$$\begin{aligned} m_R &= m_A e^{-\phi_R} \\ &= m_A (1 + z_S), \end{aligned} \quad (17)$$

which is a redshift relation connecting the mass per baryon at the surface of the star with the baryonic mass m_A taken as a reference mass by a distant observer. Once m_A is given, we obtain m_R by measuring z_S . On the other hand, inside the star, the energy density $\varepsilon(r)$, the baryonic number density $n_A(r)$, and the baryonic mass per baryon $m(r)$ decrease from the center to the surface of the star. Thus, the inequalities $m_C > m_R > m_A$ (where $m_C \equiv m(0)$) hold in the star interior. In other words, there is anomalous mass defect when $m(r) > m_A, \forall r \in [0, R]$. If $m_R \rightarrow m_A$ then the point **3** goes to the origin of the M vs. N_A plot in panel(b) indicating the absence of the anomalous mass defect when $m_R = m_A$, in the first branch of the stellar sequences, as shown in Refs. [1–4, 23]. Moreover, for a given EoS characterized by the model parameters V_1 and G_2 , m_R is constant for all stars along the corresponding stellar sequence. The slope $m_R e^{\phi_R}$ in Eq.(16) evolves along the stellar sequence being greater than m_A at the origin of the sequence and less than m_A everywhere above the point **3**. The mass defect $|\Delta_2 M|$ is maximum at the point **3**, as we see by simple inspection in panel (c).

We have calculated for different values of V_1 and G_2 the maximum values of $|\Delta_2 M|$ at the point **3** by searching for points where Eq.(17) holds. The results are depicted in Fig.2. Each plot starts from the origin ($\Delta_2 M = 0$) and ends at the maximum mass value of $\Delta_2 M$ calculated in Ref.[16] where the point **3** is located also satisfying Eq.(17). In the low mass region connected by the dotted line we have $|\Delta_2 M|$ around 1×10^{53} erg. For the sake of comparison, the energies liberated in type Ia Supernovae originated by white dwarf explosions are of the order of $(1 - 2) \times 10^{51}$ erg; and in the supernova 1987A the total energy of the observed neutrinos was found to be around $\sim 3 \times 10^{53}$ erg. In this respect, explosions of strange stars with anomalous mass defects would be a possibility to be considered.

B. The Tolmann-Oppenheimer-Volkov equations

To simplify our notation let us define the dimensionless radius and mass by

$$\mathcal{X} \equiv \frac{c^2}{GM_\odot} r \quad \text{and} \quad \mathcal{Z} \equiv \frac{M(r)}{M_\odot}, \quad (18)$$

where $M(r)$ is the mass within the sphere of radius r ; and $GM_\odot/c^2 \simeq 1.5$ km. Then, the TOV equations are given by

$$\frac{d\mathcal{Z}}{d\mathcal{X}} = \eta \mathcal{X}^2 \mathcal{E}, \quad (19)$$

$$\frac{d\mathcal{P}}{d\mathcal{X}} = -\frac{(\mathcal{E} + \mathcal{P})(\mathcal{Z} + \eta\mathcal{X}^3\mathcal{P})}{\mathcal{X}^2(1 - 2\mathcal{Z}/\mathcal{X})}, \quad (20)$$

where $\eta \equiv 4\pi(GM_\odot/c^2)^3/M_\odot c^2 \simeq 0.03628 \text{ fm}^3 \text{ GeV}^{-1}$. The redshift of the spectral lines emitted from the star surface is given by

$$z_S = \frac{1}{\sqrt{1 - 2\mathcal{Z}_R/\mathcal{X}_R}}, \quad (21)$$

where $\mathcal{X}_R \equiv \mathcal{X}(r = R)$ and $\mathcal{Z}_R \equiv \mathcal{Z}(\mathcal{X}_R)$.

As the redshift has an important role in the present work, let us explore some properties which will be important in the sequel. For finite values of ε_C and p_C at the center of the star² we find

$$\left. \frac{d\mathcal{P}(\mathcal{X})}{d\mathcal{X}} \right|_{\mathcal{X}=0} = 0. \quad (22)$$

At the star surface where energy density is \mathcal{E}_R and $\mathcal{P}_R = 0$ we have

$$\begin{aligned} \left. \frac{1}{\mathcal{E}_R} \frac{d\mathcal{P}(\mathcal{X})}{d\mathcal{X}} \right|_{\mathcal{X}=\mathcal{X}_R} &= -\frac{\mathcal{Z}_R/\mathcal{X}_R}{\mathcal{X}_R [1 - 2\mathcal{Z}_R/\mathcal{X}_R]} \\ &= -\frac{z_S^2 + 2z_S}{2\mathcal{X}_R} \\ &= -\frac{(z_S^2 + 2z_S)^2}{4\mathcal{Z}_R(1 + z_S)^2}. \end{aligned} \quad (23)$$

These expressions are of general validity whatever the energy density may be constant or not. The right hand sides of Eqs. (23) are also observables quantities directly given by the measurements of the redshift z_S and the dimensionless radius \mathcal{X}_R or mass \mathcal{Z}_R .

C. Constant energy density

In the case $\mathcal{E} \equiv \mathcal{E}_C = \text{cte}$. (see Ref. [17]) we find that

$$\mathcal{Z} = \frac{1}{3}\eta\mathcal{E}_C\mathcal{X}^3, \quad (24)$$

$$\begin{aligned} \mathcal{P} &= \mathcal{E}_C \frac{\sqrt{1 - 2\mathcal{Z}/\mathcal{X}} - \sqrt{1 - 2\mathcal{Z}_R/\mathcal{X}_R}}{3\sqrt{1 - 2\mathcal{Z}_R/\mathcal{X}_R} - \sqrt{1 - 2\mathcal{Z}/\mathcal{X}}} \\ &= \mathcal{E}_C \frac{\sqrt{1 - \frac{2}{3}\eta\mathcal{E}_C\mathcal{Z}\mathcal{X}^2} - \sqrt{1 - \frac{2}{3}\eta\mathcal{E}_C\mathcal{Z}_R\mathcal{X}_R^2}}{3\sqrt{1 - \frac{2}{3}\eta\mathcal{E}_C\mathcal{Z}_R\mathcal{X}_R^2} - \sqrt{1 - \frac{2}{3}\eta\mathcal{E}_C\mathcal{Z}\mathcal{X}^2}}. \end{aligned} \quad (25)$$

² Where $\mathcal{Z}(\mathcal{X})/\mathcal{X} \rightarrow 0$ when $\mathcal{X} \rightarrow 0$.

The redshift is now given by

$$z_S = \frac{1}{\sqrt{1 - \frac{2}{3}\eta\mathcal{E}_C\mathcal{Z}_R\mathcal{X}_R^2}}. \quad (26)$$

By taking $\mathcal{X} = 0$ in Eqs. (25), the ratio $\mathcal{P}_C/\mathcal{E}_C$ at the center of the star is given by

$$\frac{\mathcal{P}_C}{\mathcal{E}_C} = \frac{z_S}{2 - z_S}. \quad (27)$$

The EoS at the center of a compact star with constant energy density can be obtained by direct measurement of the redshift of the spectral lines emitted from the star surface. By this way, we can use the redshift as a probe to give us the EoS at the center of a compact star in the $\mathcal{E} \equiv \mathcal{E}_C = \text{cte.}$ approximation. For finite $\mathcal{P}_C/\mathcal{E}_C \geq 0$, we note that $z_S < 2$, according to Eq. (11.6.20) in Ref. [26]. Additionally, we note that the above solution for $\mathcal{P}_C/\mathcal{E}_C$ does not depend on the (nuclear or strange) matter EoS. This is an interesting property to be used to test theoretical EoS models.

Low mass compact stars have been commonly accepted as those stars with masses lower than the solar mass. They are characterized by the fact that their internal energy density profiles are almost constant. The mass is calculated by the Newtonian approximation $M \simeq (4\pi/3)\varepsilon_S R^3$, where ε_S is the surface energy density, in Ref. [27]. However, not all low mass stars can be approximated by a constant internal energy density profile. For instance, for certain values of the FCM parameters V_1 and G_2 , the shape of the energy density may present a remarkable change from the center to the surface of the star. In this case, although we do not have an analogous prescription to the one given in Eq. (27), it is possible to explore the behavior of the theoretical dependence of $(\mathcal{P}/\mathcal{E})_C$ (in the framework of the FCM) as function of the redshift to find the corresponding expression for the case of non-constant energy density profile.

IV. $(\mathcal{P}/\mathcal{E})_C$ FOR NON-CONSTANT ENERGY DENSITY

Let us now try to build a representation to simulate a general case when the energy density is not constant. To this end, we first generate many (theoretical) stellar sequences each one corresponding to a different pair of parameters V_1 and G_2 . The plots of the ratios $(\mathcal{P}/\mathcal{E})_C$ vs. z_S , which results from the calculation, are shown in panel (a) of Fig. 3. We observe that all curves that start very close together from the origin, in a thin bundle of lines, deviate from

the initial direction at certain points along the bundle resembling a "cockatiel crest" at the upper parts of the figure. Moreover, the deviation points, each one corresponding to a pair (V_1, G_2) , are located at the maximum masses of the corresponding stellar sequences. Then, the lines of the "crest" that lie in the second branches (such as the one with the point **2**, in Fig. 1) of the stellar sequences are of no interest in the present work. So, by removing the lines of the "crest" at the maximum masses, we obtain a thin cloud of aligned points which converge in the low redshift region (say, $z_S \lesssim 0.1$) to the constant energy density solution given by Eq. (27), as shown in panel (b).

The next step is to represent the cloud of points by the interpolating curve given by

$$\left(\frac{\mathcal{P}}{\mathcal{E}}\right)_C = y \left(1 - \frac{9}{8}y + 2y^2\right) \quad (28)$$

where $y \equiv \mathcal{P}_C/\mathcal{E}_C$ is the constant energy density solution given by Eq. (27). The second and third coefficients on the right hand side of Eq. (28) were initially determined through best-fitting methods and then rounded in order to give an error estimate $\lesssim 4\%$ (the best we obtained after many attempts!) at an intermediate redshift range and zero errors at zero redshift and at the maximum mass redshift, as shown in panels (c) and (d). In panel (b), the solid line shows the interpolating curve extrapolated to higher redshifts to become visible. Of course, this is a model dependent procedure valid for the case of the FCM nonperturbative EoS we are considering, but with an interesting quasi-model independent feature.

Panels (c) and (d) show the fractional error of $(\mathcal{P}/\mathcal{E})_C$ as function of the redshift and the corresponding error for z_S in terms of $(\mathcal{P}/\mathcal{E})_C$ (obtained by inverting Eq. (28)), respectively, in a scale from zero to 100. So, by this way, we are able to use a redshift measurement as a probe to estimate $(\mathcal{P}/\mathcal{E})_C$ at the center of a strange star governed by the nonperturbative FCM equation of state within the errors shown in panels (c) and (d). A direct application of Eq. (28) is done in Sec. V to investigate the compact source 1E1207.4-5209.

Coming back to panel (a), the curves at the upper parts of the figure become more and more closer, but never exceeding the limiting redshift $z_S \simeq 0.51$, for stars in the second branches of the corresponding stellar sequences. On the other hand, the values of $(\mathcal{P}/\mathcal{E})_C$ at the maximum masses along the bundle of curves does not exceed a certain limit whatever the values of G_2 may be, suggesting the existence of an upper limit for $(\mathcal{P}/\mathcal{E})_C$ and a corresponding limit for G_2 according to the values of V_1 . In order to obtain the limits

for G_2 , we considered the solutions for the cases with $V_1 = 0$ (which gives the highest "crests"), and $V_1 = 0.5 \text{ GeV}$ (which gives the lowest "crests"). In panel (a) of Fig. 4, for $V_1 = 0$ the value of $(\mathcal{P}/\mathcal{E})_{C,c}$ becomes constant around 0.262 at $z_S \simeq 0.47$ (point **c** in panel (b)) for $G_2 \gtrsim 0.035 \text{ GeV}^4$. At this point we have the ratio $\mathcal{Z}_R/\mathcal{X}_R \equiv R_S/(2R) \simeq 0.27$, where $R_S = 2GM/c^2$ is the Schwarzschild radius of the star. The mass of the star is $M \simeq 0.58 M_\odot$ and its radius is $R \simeq 3.19 \text{ km} \simeq 1.85 R_S$. For $V_1 = 0.5 \text{ GeV}$, the value of $(\mathcal{P}/\mathcal{E})_{C,d}$ becomes constant around 0.24 at $z_S \simeq 0.44$ (point **d** in panel (b)), but for a too great value of G_2 , say, $\gtrsim 2.5 \text{ GeV}^4$. The corresponding mass and radius are $M \simeq 0.06 M_\odot$ and $R \simeq 0.34 \text{ km} \simeq 1.92 R_S$.

We now end this section by considering a situation given by

$$\begin{aligned} \left(\frac{\mathcal{P}}{\mathcal{E}}\right)_C &= \frac{\mathcal{Z}_R}{\mathcal{X}_R} \\ &= \frac{1}{2} \left[1 - \frac{1}{(1+z_S)^2} \right]. \end{aligned} \quad (29)$$

Panel (b) shows the plot of the right hand side of Eq. (29) together with the plots of $\mathcal{P}_C/\mathcal{E}_C$ and $(\mathcal{P}/\mathcal{E})_C$. The point **a** is located by solving the equation

$$y - \frac{1}{2} \left[1 - \frac{1}{(1+z_S)^2} \right] = 0, \quad (30)$$

from which we obtain the root $z_S \simeq 0.39$ and the corresponding ratio

$$\left(\frac{\mathcal{P}}{\mathcal{E}}\right)_{C,a} \simeq 0.24. \quad (31)$$

Although the point **a** is on the constant energy density solution of TOV equations, the value of $(\mathcal{P}/\mathcal{E})_{C,a}$ can also be obtained for certain values of V_1 and G_2 . As a result, the point **a** is on the second branches of the stellar sequences for values of the pair (V_1, G_2) between $(V_1 \simeq 0.23 \text{ GeV}, G_2 = 0.001 \text{ GeV}^4)$ and $(V_1 = 0.5 \text{ GeV}, G_2 \simeq 0.012 \text{ GeV}^4)$.

Analogously, by solving the equation

$$y(1 - \frac{9}{8}y + 2y^2) - \frac{1}{2} \left[1 - \frac{1}{(1+z_S)^2} \right] = 0, \quad (32)$$

we find the root $z_S \simeq 0.49$ and the ratio

$$\left(\frac{\mathcal{P}}{\mathcal{E}}\right)_{C,b} \simeq 0.275 \quad (33)$$

corresponding to the point **b**. This point is located on the second branches of the stellar sequences for $V_1 = 0$ and $\forall G_2 \gtrsim 0.035 \text{ GeV}^4$. The differences between the values of $(\mathcal{P}/\mathcal{E})_C$

and z_S at the points **b** and **c** are about (4-5) %; and the differences for the masses, radii and $\mathcal{Z}_R/\mathcal{X}_R$ are \lesssim (1-3) %. Then, for observations with error bars \gtrsim (4-5) % we can assume that **b** \simeq **c** (**c** is at the maximum mass) to estimate, from z_S measurements, whether an observed star is near its maximum value $(\mathcal{P}/\mathcal{E})_{C,c}$.

V. THE COMPACT STAR 1E1207.4-5209

The possible SQM composition of the compact star 1E1207.4-5209 was considered in Ref. [28]. In a mass-radius relation investigation in Ref. [29], the mass, radius and redshift of 1E1207.4-5209 were determined (by independent methods) as being $M = 0.34 \pm 0.09 M_\odot$, $R = 4.2 \pm 0.1$ km and $z_S = 0.12 - 0.23$.

By assuming the SQM composition of 1E1207.4-5209 governed by the FCM nonperturbative EoS, we now try to find the parameters V_1 and G_2 from the given astrophysical data. Because the mass, radius and redshift are related by Eq. (21) we have two independent quantities to determine the parameters. As the redshift measurement is given only within a range, we try to obtain the parameters by following two steps.

First, we take as the central value of the redshift the one calculated from the values of the above mass and radius plus their respective error bars, by using Eq. (21). Then, we here assume $z_S = 0.15_{-0.048}^{+0.057}$ to be used in our calculation. However, the measurements of M and R , which appear in the ratio M/R , are not sufficient to discriminate the values of V_1 and G_2 . Two compact stars with different masses and radii, but with the same ratio M/R , have the same redshifts. For instance, this would be the case of two stars with the same redshift, one on the $(\mathcal{P}/\mathcal{E})_C$ curve and the other on the upper "crest", as we can observe in panels (c) and (d) of Fig. 3. To avoid this ambiguity, we have attempted to explore the right hand side of Eq. (23), by saying that even when the redshifts of two different stars are the same, their radii and/or masses are not. Unfortunately, the values of $[(dp/dr)/\varepsilon]_{r=R}$ are practically constant (around -0.03741 km $^{-1}$), with a variation of $\sim 0.003\%$ within the parameter range, resulting inappropriate to our task. So, in this first attempt do determine the model parameters, we obtained a large range of values for $V_1 \in [0, 0.5]$ GeV and $G_2 \in [0.0076, 0.014]$ GeV 4 , as we see in the V_1 vs. G_2 plot depicted by the solid line in panel (b) of Fig. 5. In order to narrow the search to get better results, we use the additional observable $(\mathcal{P}/\mathcal{E})_C = 0.073_{-0.024}^{+0.029}$ (indicated by the cross **A** in panel (a)) obtained from Eq. (28) to determine the values of the parameters

V_1 and G_2 . The error bars were determined by the use of standard methods of data analysis in Refs. [30, 31]. As a result (the cross **A** in panel (b)) we obtained $V_1 = 0.44 \pm 0.11$ GeV and $G_2 = 0.0082 \pm 0.001$ GeV⁴ for the compact star 1E1207.4-5209. Then, according to these predictions, the compact star 1E1207.4-5209 is characterized by the central pressure $\mathcal{P}_C \simeq 0.12$ GeV fm⁻³ and energy density $\mathcal{E}_C \simeq 1.6$ GeV fm⁻³ $\simeq 11 \varepsilon_0$ (where $\varepsilon_0 \simeq 0.141$ GeV fm⁻³ is the nuclear energy density); the mass per baryon $m_C \simeq 1.78$ GeV $\simeq 1.89 m_A$ at $r = 0$ and $m_R \simeq 1.75$ GeV $\simeq 1.87 m_A$ at $r = R$. As a consequence of the high values of V_1 and G_2 , the predicted anomalous mass defect is $|\Delta_2 M| \simeq 2.56 \times 10^{53}$ erg.

Second, let us consider the redshift range 0.12-0.23 from which we take the redshift $z_S = 0.175 \pm 0.055$ at the central point and the respective additional observable $(\mathcal{P}/\mathcal{E})_C = 0.087 \pm 0.028$ (indicated by the cross **B** in panel (a)) obtained from Eq. (28). The dashed line in panel (b) has the same meaning as the solid line in first step. By an analogous procedure to narrow our search we obtained $V_1 = 0.43 \pm 0.085$ GeV and $G_2 = 0.0093 \pm 0.00092$ GeV⁴. In this case, the compact star 1E1207.4-5209 becomes characterized by the central pressure $\mathcal{P}_C \simeq 0.17$ GeV fm⁻³, energy density $\mathcal{E}_C \simeq 1.95$ GeV fm⁻³ $\simeq 14 \varepsilon_0$; the mass per baryon $m_C \simeq 1.81$ GeV $\simeq 1.93 m_A$ at $r = 0$ and $m_R \simeq 1.77$ GeV $\simeq 1.88 m_A$ at $r = R$. The corresponding anomalous mass defect is $|\Delta_2 M| \simeq 2.94 \times 10^{53}$ erg.

In both steps considered above, it is a remarkable feature of the FCM that the determination of the $q\bar{q}$ interaction potential from astrophysical observations is in good agreement with $V_1 = 0.5$ GeV provided by lattice calculations in Ref.: [32]. However, the values of G_2 are $\sim 20\%$ above $G_2 = 0.00682$ GeV⁴ (predicted in Ref. [15]) in the first step and above $\sim 36\%$ in the second step. Finally, we observe that the values of $|\Delta_2 M|$ are not in contradiction with the results shown in Fig. 2. The star 1E1207.4-5209 is not at the maximum mass nor at the point **3** of the stellar sequence corresponding to the above values of V_1 and G_2 .

VI. FINAL REMARKS

In the present work, we addressed the question of anomalous mass defects of low mass strange stars in the framework of the Field Correlator Method (FCM). Redshift measurements played an important role in the determination of the model parameters from astrophysical observations. In the case of the constant energy density solution of Tolmann-Oppenheimer-Volkov equations, the ratio $(\mathcal{P}/\mathcal{E})_C$ at the center of a compact star was an

important observable quantity determined directly by redshift measurements. It tells us how the equation of state at $r = 0$ is.

In the general case, when the energy density is not constant, we verified that the plots of $(\mathcal{P}/\mathcal{E})_C$ vs. redshift, for different values of the model parameters V_1 e G_2 , are concentrated in a thin region with a quasi linear behavior, ranging from the origin to the maximum masses in the first branches of the stellar configurations. This fact enabled us to build a representation for the ratio $(\mathcal{P}/\mathcal{E})_C$ in terms of the redshift similar to the one for the case of constant energy density. A remarkable feature of the approach is that the ratio $(\mathcal{P}/\mathcal{E})_C$ as function of the redshift present the lowest values with respect to other models of nuclear matter. For instance, as illustrated in Fig. 6 for the Walecka nuclear mean field theory in Refs. [33, 34], our preliminary calculations have shown that the values of $(\mathcal{P}/\mathcal{E})_C \forall z_S \in [0, 0.5]$, are in the intermediate region between the solution for constant energy density and the one corresponding to the SQM in the FCM framework. However, for different values of the two coupling constant g_σ/m_σ and g_ω/m_ω of the nuclear mean field theory the curves of $(\mathcal{P}/\mathcal{E})_C$ (in the redshift range we are considering) are not concentrated in a line of points as they are for the MFC. An interesting task to be considered in future works is the investigation of the behavior of the ratio $(\mathcal{P}/\mathcal{E})_C$ provided by other models of nuclear matter in the framework of mean field theories. Our attempt to determine ratio $(\mathcal{P}/\mathcal{E})_C$ in terms of the redshift is model dependent, but with an almost model independent feature. It is important to verify in future works whether this feature remains valid for other approaches used to describe SQM.

ACKNOWLEDGMENTS

This work was done with the support provided by the Ministério da Ciência , Tecnologia e Inovação (MCTI).

-
- [1] V. A. Ambartsumyan, G. S. Saakyan, Sov. Astron -AJ 4 (1960) 187.
 - [2] V. A. Ambartsumyan, G. S. Saakyan, Sov. Astron -AJ 5 (1962) 601.
 - [3] V. A. Ambartsumyan, G. S. Saakyan, Sov. Astron -AJ 5 (1962) 779.
 - [4] G. S. Saakyan, Yu. L. Vartanyan, Sov. Astron.-AJ 8 (1964) 147.
 - [5] V. A. Ambartsumyan, Problemes de la Cosmogonie Contemporaine, Editions MIR, Moscou,

- 1971.
- [6] N. Itoh, Prog. Theor. Phys. 44 (1970) 291.
 - [7] A. R. Bodmer, Phys. Rev. D4 (1971) 1601.
 - [8] H. Terazawa, INS-Report-336 (INS, University of Tokyo, Tokyo) May, 1979.
 - [9] E. Witten, Phys. Rev. D30 (1984) 272.
 - [10] E. Farhi, R. L. Jaffe, Phys. Rev. D30 (1984) 2379.
 - [11] C. Alcock, E. Farhi, A. Olinto, Astrophys. J. 310 (1986) 261.
 - [12] P. Haensel, J. L. Zdunik, R. Schaeffer, Astron. Astrophys. 160 (1986) 121.
 - [13] M. Sinha, Xu-Guang Huang, A. Sedrakian, Phys. Rev. D88 (2013) 025008.
 - [14] J. L. Richardson, Phys. Lett. B82 (1979) 272.
 - [15] Yu. A. Simonov, Ann. Phys. 323 (2008) 783.
 - [16] F. I. M. Pereira, Nucl. Phys A 953 (2016) 65.
 - [17] S. L. Shapiro, S. A. Teukolski, Black Holes, White Dwarfs and Neutron Stars, John Wiley and Sons, New York, 1983.
 - [18] F. I. M. Pereira, Nucl. Phys A 860 (2011) 102.
 - [19] F. I. M. Pereira, Nucl. Phys A 897 (2013) 151.
 - [20] Yu. A. Simonov, M. A. Trusov, JETP Lett. 85 (2007) 598.
 - [21] Yu. A. Simonov, M. A. Trusov, Phys. Lett. B650 (2007) 36.
 - [22] N. Glendenning, Compact Stars, Nuclear Physics, Particle Physics, and Relativity, Springer, New York, 2000, 2nd ed..
 - [23] Ya. B. Zel'dovich and I. D. Novikov, Stars and Relativity, Dover Publications, Inc., Mineola, New York, 1996.
 - [24] Yu. L. Vartanyan, A. R. Arutyunyan, A. K. Grigoryan, Astrophysics 37 (1994) 271.
 - [25] Yu. L. Vartanyan, A. K. Grigoryan, G. A. Khachatryan, Astrophysics 38 (1995) 152.
 - [26] S. Weinberg, Gravitation and Cosmology, John Wiley & Sons, New York, 1972.
 - [27] Haensel, Potenkin and Yakovlev, Neutron Stars 1, Equation of State and Structure, Springer, New York, 2007.
 - [28] R. X. Xu, Mon. Not. R. Astron. Soc. 356 359 (2005).
 - [29] C. M. Zhang, H. X. Yin, Y. Kojima, H. K. Chang, R. X. Xu, X.-D. Li, B. Zhang, B. Kiziltan, Mon. Not. R. Astron. Soc. 374 232 (2007) 232.
 - [30] P. R. Bevington, Data Reduction and Error Analysis for the Physical Sciences, McGraw-Hill

Book Company, New York, 1969.

- [31] P. R. Bevington, D. K. Robinson, Data Reduction and Error Analysis for the Physical Sciences, McGraw-Hill Higher Education, New York, 2003.
- [32] O.Kaczmarek, F. Zantov, arXiv:hep-lat/0506019.
- [33] J. D. Walecka, Ann. Phys. **83** (1974) 491.
- [34] B. D. Serot, J.D. Walecka, Advances in Nuclear Physics **16**, Plenum Press, 1986.

FIGURE CAPTION

Fig. 1 - For the given values of G_2 (in GeV^4 units) and V_1 (in GeV units): panel (a), gravitational mass M and baryonic mass M_A as function of the central density; panel (b), gravitational mass M and baryonic mass M_A as function of the baryonic number N_A ; panel (c), mass defect as function of the gravitational mass M . Labels **1** and **2** indicate the points at which $M = M_A$ and where the solid curve and dashed curve cross itself, in panel (b).

Fig. 2 - The mass defect $\Delta_2 M$ as function of G_2 for different values of V_1 between $V_1 = 0$ and $V_1 = 0.5$ GeV. The labels correspond to the values of V_1 (in GeV units). *Solid lines*: $\Delta_2 M$ at the point **3** obtained by Eq. (17). *Short dashed lines*: $\Delta_2 M$ at the maximum masses of the stellar configurations (cf. Fig. 4 in Ref. [16]). *Dotted lines*: $\Delta_2 M$ at the point **3** of the low stellar masses ranging from $M/M_\odot \simeq 0.6$ at $V_1 = 0$ to $M/M_\odot \simeq 1.1$ at $V_1 = 0.3$ GeV. *Long dashed lines*: only connecting points of $\Delta_2 M$ when the point **3** is at the maximum mass.

Fig. 3 - Panel (a): for the given ranges of G_2 (in GeV^4 units) and V_1 (in GeV units), the ratio $(\mathcal{P}/\mathcal{E})_C$ at $r = 0$ as function of the redshift. The values of V_1 increase from top to bottom. The values of G_2 increase from bottom to top. Panel (b): as in panel (a), but for values of $(\mathcal{P}/\mathcal{E})_C$ ending at the maximum masses of the stellar configurations. *Short dashed line*: $\mathcal{P}_C/\mathcal{E}_C$ corresponding to the energy solution of the TOV equations given by Eq. (27). *Solid line*: the interpolating curve given by Eq. (28). Panel (c): the fractional error $\delta(\mathcal{P}/\mathcal{E})_C / (\mathcal{P}/\mathcal{E})_C$ as function of the redshift. Panel (d): as in panel (c), but for $\delta z_S / z_S$.

Fig. 4 - As in panel (b) of figure 3, but including the $\mathcal{Z}_R/\mathcal{X}_R$ plot (long dashed line). The label **a** corresponds to Eq. (31) and the label **b** corresponds to Eq. (33). The label **c** indicates the upper bound $(\mathcal{P}/\mathcal{E})_{C,c} \simeq 0.262$ and the corresponding redshift $z_S \simeq 0.47$. Panel (b): for increasing values of G_2 , the "constancies" of $(\mathcal{P}/\mathcal{E})_C$ at **b**, **c** and **d** (not visible in the scale of the figure).

Fig. 5 - Panel (a): as in panel (b) of Fig. 3, but without the cloud of points. The cross **A** indicates the value of $(\mathcal{P}/\mathcal{E})_C = 0.073_{-0.024}^{+0.029}$ calculated by Eq. (28) corresponding to the redshift $z_S = 0.15_{-0.048}^{+0.057}$. The cross **B** indicates the value of $(\mathcal{P}/\mathcal{E})_C = 0.087 \pm 0.028$ calculated by Eq. (28) corresponding to the redshift $z_S = 0.175 \pm 0.055$. Panel (b): the solid and dashed lines show the first attempts to determine the model parameters V_1 and G_2 from the mass, radius and redshift measurements provided by the observations of the compact star 1E1207.4-5209. The crosses **A** and **B** indicate the final results of our narrowed searches

for V_1 and G_2 . For comparison, the dashed line at $V_1 = 0.5$ GeV displays the result obtained from lattice calculations, in Ref.: [32].

Fig. 6 - The ratios pressure to energy density at $r = 0$: (a) *Solid lines*, $\mathcal{P}_C/\mathcal{E}_C$ and $(\mathcal{P}/\mathcal{E})_C$ given by Eqs. (27) and (28); (b) *Short dashed line*, for the nuclear mean field theory, with the coupling constants $(g_\sigma/m_\sigma)^2 = 11.798 \text{ fm}^2$ and $(g_\omega/m_\omega)^2 = 8.653 \text{ fm}^2$ fixed to give the bind energy $E_b = -15.75 \text{ MeV}$ and $k_F = 1.42 \text{ fm}^{-1}$; (c) *Long dashed line*, as in (b) but for the arbitrarily chosen values of $(g_\sigma/m_\sigma)^2 = 15.0 \text{ fm}^2$ and $(g_\omega/m_\omega)^2 = 12.0 \text{ fm}^2$, as functions of the surface redshift.

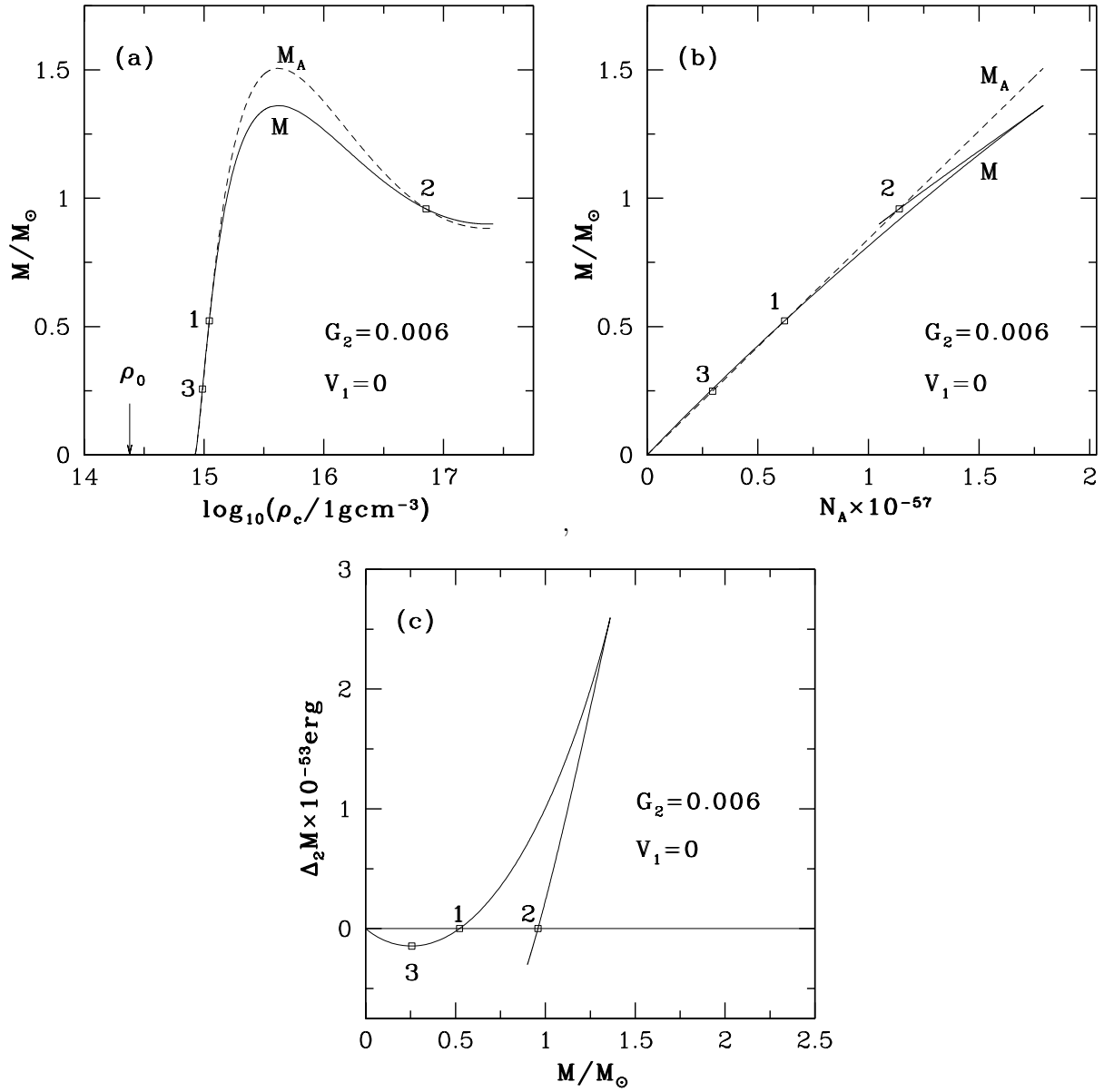


FIG. 1. For the given values of G_2 (in GeV^4 units) and V_1 (in GeV units): panel (a), gravitational mass M and baryonic mass M_A as function of the central density; panel (b), gravitational mass M and baryonic mass M_A as function of the baryonic number N_A ; panel (c), mass defect as function of the gravitational mass M . Labels **1** and **2** indicate the points at which $M = M_A$ and where the solid curve and dashed curve cross itself, in panel (b).

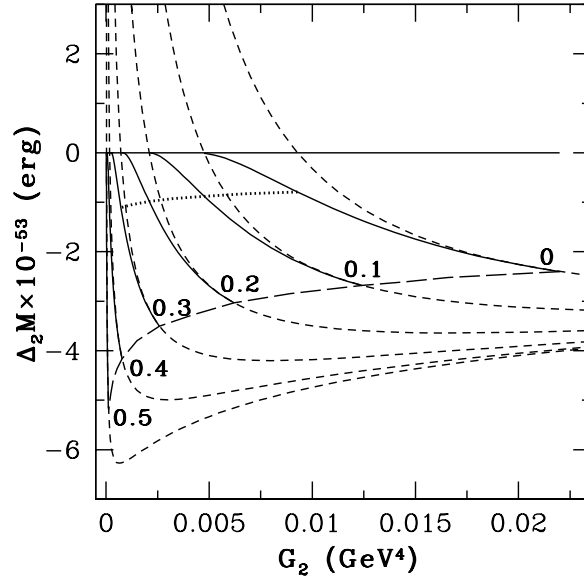


FIG. 2. The mass defect $\Delta_2 M$ as function of G_2 for different values of V_1 between $V_1 = 0$ and $V_1 = 0.5$ GeV. The labels correspond to the values of V_1 (in GeV units). *Solid lines*: $\Delta_2 M$ at the point **3** obtained by Eq. (17). *Short dashed lines*: $\Delta_2 M$ at the maximum masses of the stellar configurations (cf. Fig. 4 in Ref. [16]). *Dotted lines*: $\Delta_2 M$ at the point **3** of the low stellar masses ranging from $M/M_\odot \simeq 0.6$ at $V_1 = 0$ to $M/M_\odot \simeq 1.1$ at $V_1 = 0.3$ GeV. *Long dashed lines*: only connecting points of $\Delta_2 M$ when the point **3** is at the maximum mass.

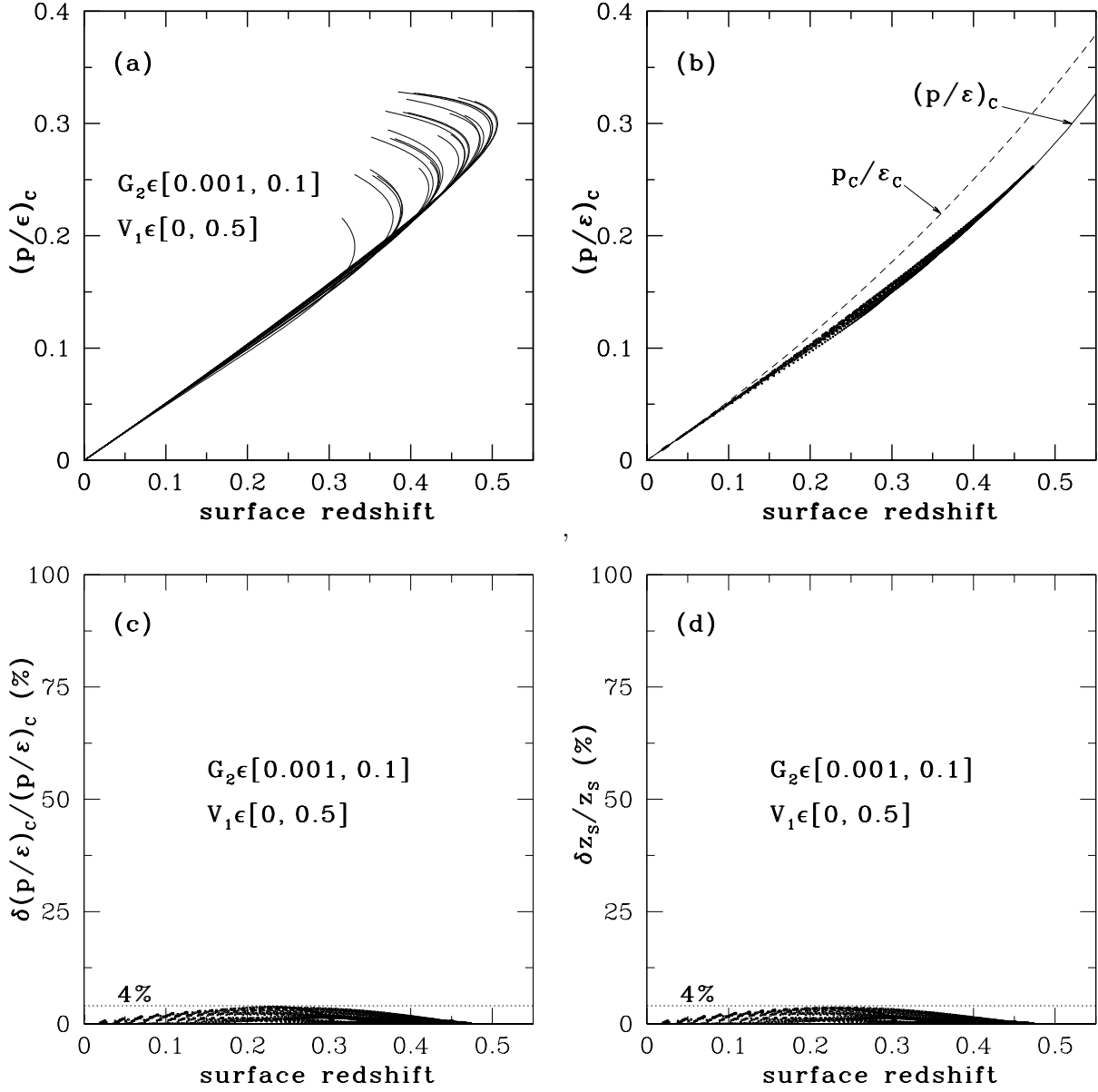


FIG. 3. Panel (a): for the given ranges of G_2 (in GeV^4 units) and V_1 (in GeV units), the ratio $(\mathcal{P}/\mathcal{E})_C$ at $r = 0$ as function of the redshift. The values of V_1 increase from top to bottom. The values of G_2 increase from bottom to top. Panel (b): as in panel (a), but for values of $(\mathcal{P}/\mathcal{E})_C$ ending at the maximum masses of the stellar configurations. *Short dashed line*: $\mathcal{P}_C/\mathcal{E}_C$ corresponding to the energy solution of the TOV equations given by Eq. (27). *Solid line*: the interpolating curve given by Eq. (28). Panel (c): the fractional error $\delta(\mathcal{P}/\mathcal{E})_C / (\mathcal{P}/\mathcal{E})_C$ as function of the redshift. Panel (d): as in panel (c), but for $\delta z_S / z_S$.

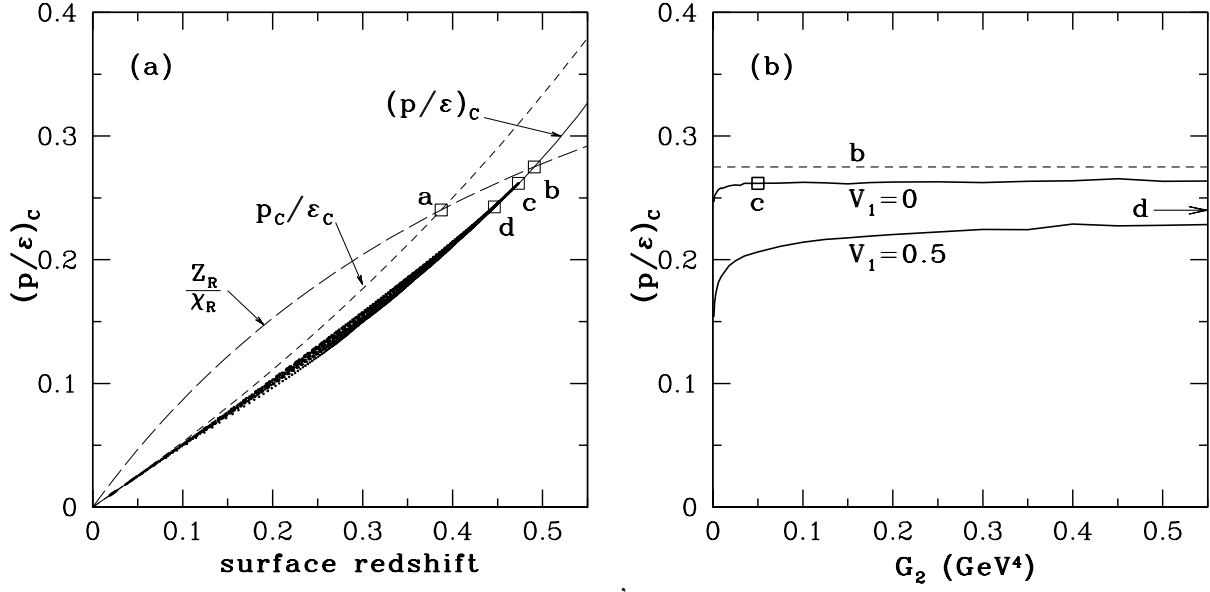


FIG. 4. As in panel (b) of figure 3, but including the $\mathcal{Z}_R/\mathcal{X}_R$ plot (long dashed line). The label **a** corresponds to Eq. (31) and the label **b** corresponds to Eq. (33). The label **c** indicates the upper bound $(\mathcal{P}/\mathcal{E})_{C,c} \simeq 0.262$ and the corresponding redshift $z_S \simeq 0.47$. Panel (b): for increasing values of G_2 , the "constancies" of $(\mathcal{P}/\mathcal{E})_C$ at **b**, **c** and **d** (not visible in the scale of the figure).

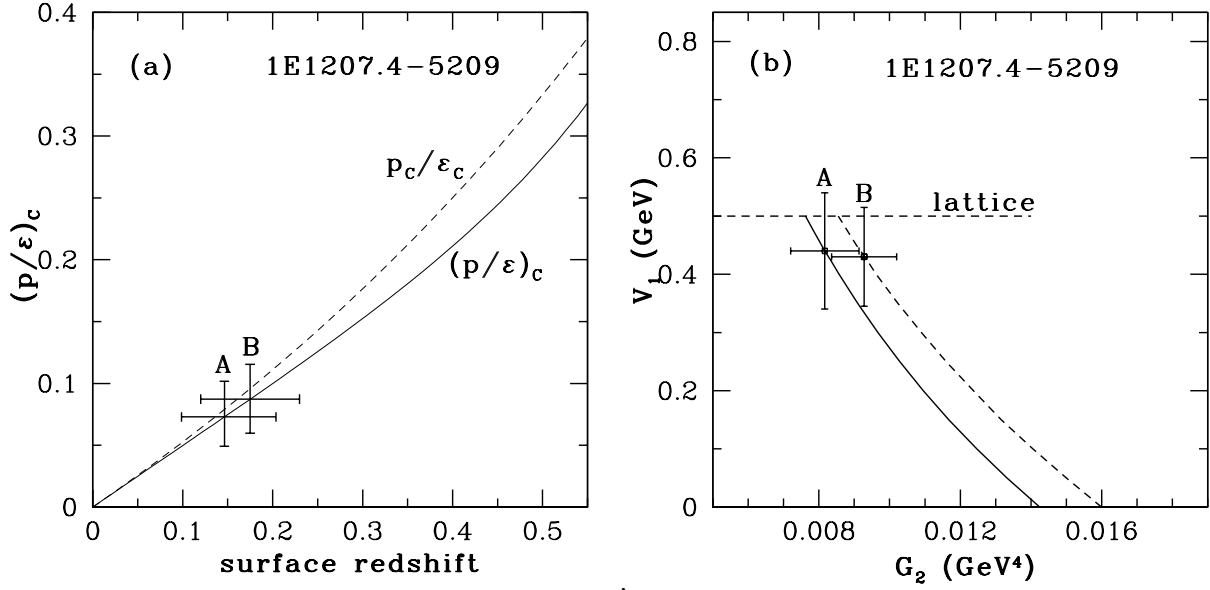


FIG. 5. Panel (a): as in panel (b) of Fig. 3, but without the cloud of points. The cross **A** indicates the value of $(\mathcal{P}/\mathcal{E})_C = 0.073^{+0.029}_{-0.024}$ calculated by Eq. (28) corresponding to the redshift $z_S = 0.15^{+0.057}_{-0.048}$. The cross **B** indicates the value of $(\mathcal{P}/\mathcal{E})_C = 0.087 \pm 0.028$ calculated by Eq. (28) corresponding to the redshift $z_S = 0.175 \pm 0.055$. Panel (b): the solid and dashed lines show the first attempts to determine the model parameters V_1 and G_2 from the mass, radius and redshift measurements provided by the observations of the compact star 1E1207.4-5209. The crosses **A** and **B** indicate the final results of our narrowed searches for V_1 and G_2 . For comparison, the dashed line at $V_1 = 0.5$ GeV displays the result obtained from lattice calculations, in Ref.: [32].

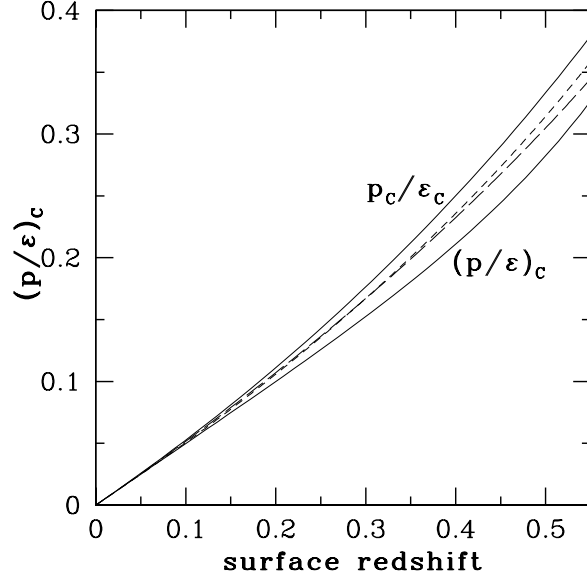


FIG. 6. The ratios pressure to energy density at $r = 0$: (a) *Solid lines*, $\mathcal{P}_C/\mathcal{E}_C$ and $(\mathcal{P}/\mathcal{E})_C$ given by Eqs. (27) and (28); (b) *Short dashed line*, for the nuclear mean field theory, with the coupling constants $(g_\sigma/m_\sigma)^2 = 11.798 \text{ fm}^2$ and $(g_\omega/m_\omega)^2 = 8.653 \text{ fm}^2$ fixed to give the bind energy $E_b = -15.75 \text{ MeV}$ and $k_F = 1.42 \text{ fm}^{-1}$; (c) *Long dashed line*, as in (b) but for the arbitrarily chosen values: $(g_\sigma/m_\sigma)^2 = 15.0 \text{ fm}^2$ and $(g_\omega/m_\omega)^2 = 12.0 \text{ fm}^2$, as functions of the surface redshift.